BILINGUAL PUBLISHING GROUP

Journal of Atmospheric Science Research

https://journals.bilpubgroup.com/index.php/jasr

ARTICLE

Case Study of Coastal Fog Events in Senegal Using LIDAR Ceilometer

Semou Ndao[1*], Cheikh Modou Noreyni Fall[1], Luis Durán[2], Assie Regina Djiguene Diatta[1,3], Abdou lahat Dieng[1], Badara Sane[1,4], Amadou Thierno Gaye[1]

[1] Laboratory of Physics of the Atmosphere and Ocean-Siméon Fongang (LPAO-SF), Higher Polytechnic School, University Cheikh Anta Diop (UCAD), PO BOX 5085, Dakar, Senegal

[2] Department of Earth Physics and Astrophysics, Complutense University of Madrid, Madrid, 28040, Spain

[3] Meteorological Operation Service, Representation of the Agency for the Safety of Air Navigation in Africa and Madagascar (ASECNA) in Senegal, PO BOX 3144, Dakar, Senegal

[4] Laboratory of Oceanography and Climate, Experiments and Numerical Approaches (LOCEAN), Sorbonne University (SU), Paris, 75006, France

ABSTRACT

This study aims to examine the atmospheric conditions characterising fog phenomena on the Senegalese coast focusing on two specific instances that occurred on April 3 and April 30, 2023. These events were detected by the LIDAR Ceilometer installed at LPAOSF/ESP/UCAD and confirmed on the METARs of the meteorological stations at Dakar and Diass airports. The LIDAR's backscatter signal showed that the fog of April 3 started around midnight with a vertical extension at 100 m altitude and dissipated around 10 a.m. The April 30 event characterized by a good vertical extension from the surface up to 300 m above sea level, was triggered just after 2 a.m. and lasted around 3 hours. The results showed that a decrease in temperature, accompanied by an increase in humidity and light wind, is favorable for the triggering and persistence of fog. Sea Level Pressure (SLP) anomaly fields show two distinct configurations. The April 3 event was characterized by a zonal dipole of SLP anomalies between the Sahara and the northern Senegalese coast, while the April 30 event was characterized by a meridional dipole between the Sahara and the Gulf of Guinea area as far as the equatorial Atlantic. A weakening of the pressure around the study area was observed in both cases, allowing moisture advection to favor the onset of fog. The hovmoller diagrams of relative humidity and wind show that a good vertical extension of humidity associated with a westerly wind in the lower layers plays an important role in the formation and persistence of fog. The presence of dry air associated with a weak easterly wind in the middle layers could explain the low vertical extension of the fog on April 3. A strong wind in the lower layers would be responsible for the premature dissipation of the April 30 fog.

Keywords: Coastal fog; LIDAR; Ceilometer; Sea level pressure; Relative humidity; Temperature

*CORRESPONDING AUTHOR:

Semou Ndao, Laboratory of Physics of the Atmosphere and Ocean-Siméon Fongang (LPAO-SF), Higher Polytechnic School, University Cheikh Anta Diop (UCAD), PO BOX 5085, Dakar, Senegal; Email: semoundao2@gmail.com; semou1.ndao@ucad.edu.sn

ARTICLE INFO

Received: 2 September 2023 | Revised: 11 October 2023 | Accepted: 18 October 2023 | Published Online: 27 October 2023

DOI: https://doi.org/10.30564/jasr.v6i4.5943

CITATION

Ndao, S., Fall, C.M.N., Durán, L., et al., 2023. Cases Study of Coastal Fog Events in Senegal Using LIDAR Ceilometer. Journal of Atmospheric Science Research. 6(4): 64-76. DOI: https://doi.org/10.30564/jasr.v6i4.5943

1. Introduction

According to the World Meteorological Organization (WMO), fog is defined as a suspension of fine water droplets near the ground, which can reduce horizontal visibility to less than one kilometer [1]. Fog events can have significant impacts on key sectors of the economy such as transport and agriculture [2], which are already highly dependent on climate in Sahelian countries like Senegal [3]. Fog events can buffer the summer dry season through shading effects and direct water inputs for economically important crops. For the transport sector, these impacts may be harmful. When fog is thick, it creates a sensation of an empty field due to a lack of visual cues, leading to a misjudgment of speeds and distances [4]; it is the inadequacy of these two parameters that causes almost all accidents in foggy weather. In the air transport sector, fog is one of the most dangerous phenomena for aviation, particularly during the take-off and landing phases. The deadliest air accident in the history of civil aviation, with 583 victims, took place on March 27, 1977, due to thick fog at Tenerife airport in the Canary Islands. In France, the Meuse Valley fog of December 1930, still known as Deadly fog of Meuse's valley, claimed dozens of lives [5].

Its hazardous nature for aviation has prompted developed countries to equip themselves not only with suitable observation and monitoring equipment to better understand the "life cycle" of fogs, from their formation to their dissipation, but also for forecasting purposes. Unfortunately, developing countries such as Senegal find it difficult to understand, monitor and predict these phenomena, due to their poor climatic observation infrastructure. However, researchers in the South are increasingly beginning to focus on this phenomenon in order to better characterize it. With this in mind, the Laboratory of Physics of the Atmosphere and Ocean at UCAD's Higher Polytechnic school with the help of Universidad Complutense of Madrid installed a VAISALA LIDAR CL31 in April 2012 to monitor the atmospheric conditions that cause fog. This sensor is nowadays part of UCadMet observatory which is supported and maintained by both institutions. Previous studies have highlighted the need for detailed in situ and remote sensing observations of environmental, microphysical and dynamic processes on multiple spatio-temporal scales to improve fog understanding and predictability [6]. Kim and Yum (2010) mention that fogs, forming over coastal regions, can be classified into two categories: 1) coastal fogs, which form directly over the mainland and their extension is limited to these regions, and 2) marine fogs, which develop in the open ocean and can extend or move towards coastal regions [7]. The sea fogs studied are often of three types: advection, sea smoke and fog resulting from stratus subsidence. Advection fog forms when an atmospheric boundary layer, generally well mixed, is advected onto a colder surface (snow or ice surface, cold water surface) [8]. It is linked to the cooling of the atmosphere on contact with this cold surface, which propagates by turbulence into the neighbouring layers, leading to the condensation of water vapour if the atmosphere is sufficiently humid. Sea-smoke fog generally forms in winter, over a pond or river, when cold air overcomes a warmer water surface [9]. This type of fog is associated with the evaporation of liquid water. Indeed, the difference in vapor pressure between the air and the water surface leads to evaporation, and then the mixing of the water vapor in the cold air leads to super-saturation and consequently to the formation of fog. Concerning coastal fogs, which form directly on the continental part of coastal regions and their extension is limited to these regions [10]. Ryznar (1977) has shown that advection-radiation fog is a coastal phenomenon that results from the radiative cooling of moist air that has been advected onto the continent from the ocean or from a large body of water during the afternoon [11-13]. The dynamic and thermodynamic processes underlying various mechanisms differ, and environmental and microphysical conditions determine which type of fog may appear. Fernando et al. (2020) and Bardoel et al. (2021) identified a case where turbulent mixing between nearly saturated air masses of different temperatures (e.g., a colder gravity current under warmer air) is associated with coastal topography producing

fog [14,15]. One of the most frequently studied coastal fog is advection fog. Choi and Speer (2006) analyzed and described the physical mechanisms leading to the formation of advection fog through a case study on the Yellow Sea, near the Korean coast [16]. These authors have shown that the landforms that delimit this coastal region influence the process of fog formation on the coast in combination with the breeze cycle. These studies confirm that the fogs studied in coastal areas are influenced by several factors on different spatio-temporal scales (advective transport, turbulent exchanges, relief, etc.). Geographically, scientific research on coastal fog has focused more on the American, English, Chinese, Korean and Japanese coasts. This research has focused in particular on the north coast of Scotland and the west coast of California [17-21]. Other studies have focused on the analysis of sea fog in the eastern part of Asia near China, in particular the Yellow Sea [22-24]. Heo et al. (2010) studied fogs of interest on the Korean coast [9]. However, the coastal areas of the eastern North Atlantic that experience a high frequency of fog are little studied in detail, such as the northwest coast of Senegal. Hence the interest in conducting this study to better understand the specificity of the factors controlling the development of these phenomena.

In this study, we focus on the fog events that affected the extreme west coast of Senegal on April 3 and 30 in 2023. The aim of this study is to characterize these two fog events, which respectively caused a fatal road accident on the Dakar freeway and aircraft diversions at Diass airport. The analysis of these two events is based on in situ observations, such as LIDAR from LPAOSF and METAR data from Yoff and Diass airports. The synoptic conditions associated with the formation of these phenomena were analyzed using ERA5 reanalyses. Section 2 describes the data used and the methodological approach adopted. Section 3 presents the results, followed by a discussion. Section 4 presents the main conclusions of the study.

2. Data and methodology

2.1 Data

In order to characterize the two fog events observed in Dakar on April 3 and 30, 2023, we used several types of data, namely lidar data, in situ observations and reanalyses. The LIDAR data used in this work come from VAISALA's CL31 Ceilometer (17.46°W, 14.68 °N). This instrument was installed 20 m above ground on the roof of the Laboratory of Physics of the Atmosphere and Ocean (LPAO) of Cheikh Anta Diop University (UCAD) in April 2012 thanks to the collaboration with Complutense University of Madrid (UCM, Spain) and interMET SME. The acquisition of this device was made possible thanks to a collaboration between Howard University and UCAD through LPAO-SF. This LIDAR is now part of a climate observatory: UCadMet (https://ucadmet.net) named after the two supporting institutions: UCAD and UCM. The operation of the Vaisala CL31 ceilometer is based on an InGaAs laser diode, sending pulses along the zenith direction with an energy per pulse of 1.2 μJ ± 20% [25,26]. This laser diode is eye-safe at a wavelength of 905 nm. The ceilometer uses a single-lens system with overlapping transmit and receive optics. This beam overlap occurs at shallower altitudes, providing an almost complete overlap of the transmitter and receiver field of view at altitudes above 30 m [26]. An inclined mirror separates the transmitting and receiving zones, with a hole in the center. The half-angle beam divergence for our ceilometer measures 0.75 milliradians (mrad) and has 0.66 mrad for the half-angle field of view. This LIDAR has a measurement range from 0 to 7500 m asl, with high temporal resolution (16 seconds, 5400 profiles per day) and high vertical resolution (10 m).

All the technical properties of the LIDAR ceilometer used for this study are summarized in **Table 1** [25,26].

This ceilometer combined with the Boundary

Table 1. Technical properties of VAISALA's CL31.

Property	Value
Laser system	Indium Gallium Arsenide pulsed diode laser
wavelength	905 nm
Pulse properties	1.2 μJ ± 20%
half-angle beam divergence	0.75 milliradian (mrad)
half-angle field of view	0.66 mrad
Measurement range	0-7500 m
Vertical resolution	10 m
Temporal resolution	16 seconds, 5400 profiles per day

Layer View (BL-View) software provides a good vertical profile of the attenuated backscatter signal of atmospheric particles. Several variables are measured, mainly cloud base height, mixing layer level, reflectivity, vertical visibility, atmospheric aerosol load and others [27].

The meteorological observation data used here come from the UCadMet meteorological network and METARs. The UCadMet network, set up in 2012, is the result of various measurement efforts carried out in recent years, mainly thanks to LPAO-SF, UCM and interMET (InterMET Sistemas y Redes S.L.U., Spain). The network is based on automatic weather stations located at a number of sites in the Dakar region. This area extends from the ESP (UCAD) to the island of Gorée. A very heterogeneous area of several kilometers is covered, with a mixture of suburban, urban, rural and maritime environments. Data are sampled every second, then 10-minute averages, maximums, minimums and standard deviation are calculated over a 10-minute integration period. Atmospheric data collected include air temperature at 2 meters height (°C), relative humidity at 2 meters height (%), wind speed at 4 meters height (m/s), and mean wind direction at 4 meters height. Data is periodically checked by visual inspection, and performance reports are produced every three months.

The Meteorological Aerodrome Report (METAR) data used in this work are from Yoff airport (14.73 N-17.50 W) and Diass airport (14.67 N-17.07 W). A METAR is a weather bulletin with a frequency of 30 min or less, mainly used by pilots as part of a pre-flight weather briefing, and by meteorologists, who use aggregated METAR information to aid weather forecasting. Raw METAR is the world's most common format for the transmission of meteorological observation data. It is strongly regulated by the International Civil Aviation Organization (ICAO), which means that it is understood in most parts of the world. A typical METAR contains data on temperature, dew point, wind speed and direction, precipitation, cloud cover, precipitation, cloud cover and height, visibility and barometric pressure. A METAR may also contain information on precipitation amounts, lightning and other information of interest to pilots or meteorologists, such as a pilot report or PIREP, color states and runway visual range (RVR).

In addition to observational data, we also used reanalysis data from ERA5. ERA5 is the fifth generation of European Centre for Medium-Range Weather Forecasts (ECMWF) atmospheric global climate reanalyses, produced by assimilating several satellite and radiosonde observational datasets [28]. It also includes various observational data sets obtained from the WMO's Global Telecommunications System (GTS). The spatial resolution of the data is 0.25° × 0.25° (around 28 km), with 27 pressure levels between 100 and 1000 hPa, including around seven levels in the lowest 1.5 km. Hourly relative humidity and wind are used at different levels to characterize the synoptic environment over Dakar during the fog events studied. Sea Level Pressure (SLP) was also used to monitor the land-sea thermal contrast.

2.2 Methodology

In this study, the fog events that occurred on April 3 and 30, 2023 were detected from the LIDAR backscatter signal. A ceilometer sends out short, powerful laser pulses in a vertical or near-vertical direction. The reflection of light caused by haze, fog, precipitation, aerosols and clouds, known as backscatter, is measured in units of 10^{-9} m^{-1} sr^{-1}. The backscatter signal is generally stronger in the planetary boundary layer where particle concentration is higher, but weaker in the free atmosphere where the atmosphere generally contains fewer particles. BL-View detects the backscatter gradient between the planetary boundary layer and the free atmosphere (the mixing height), as well as other atmospheric structures, such as residual boundary layers and high smoke or aerosol plumes, which can produce strong backscatter gradients. BL-view expresses the intensity of the backscatter signal using color codes for the detection of meteorological phenomena. The color red indicates a signal from clouds, precipitation and fog, and if the color is light blue to yellow, it's an aerosol backscatter signal. To reduce sensitivity to noise and transient details of atmospheric structure, BL-view performs vertical and temporal averaging on ceilometer data. Long averaging intervals avoid false gradient minima generated by signal noise. However, this approach reduces the algorithm's ability to respond to short-scale signal fluctuations in space and time. The level of signal noise depends on range and time of day. The gradient method allows the averaging parameters to be varied. To better determine the spatial expansion of fog events, we compared meteorological parameters such as air temperature, dew point temperature and relative humidity at the three sites of UCAD, Diass and Yoff airports. The dew point temperature at the LIDAR site was calculated using Equation (1) from the relative humidity measured by the UCadMet station [29].

$$T_d = \frac{243.04\left(ln\left(\frac{\mathrm{RH}}{100}\right)+\frac{17.625T}{243.04+T}\right)}{17.625-\left(ln\left(\frac{RH}{100}\right)+\frac{17,625T}{243,04+T}\right)} \quad (1)$$

where T_d is the dew point temperature (in degrees Celsius), T is the Temperature in degrees Celsius and RH is the relative humidity of the air (in percent).

As the relative humidity is not provided directly by the METAR, we calculated it from the dew point temperature using Equation (2) [29].

$$RH = \frac{p_w}{p_s} * 100 \quad (2)$$

where P_w is the ambient vapor pressure and p_s is the saturation water vapor pressure. They are given by the following Equations (3) and (4) [29]:

$$Ps = 6.112 * e^{\frac{17.67T}{(T+243,5)}} \quad (3)$$

$$Pw = 6.112 * e^{\frac{17.67T_d}{(T_d+243,5)}} \quad (4)$$

The following criterion was applied to these meteorological parameters to detect fog events. Indeed, if the relative humidity is above 90% for more than six hours and the weather is marked as fog but not rain or snow, the period is selected as a fog episode [30]. After characterizing the two fog events in terms of duration and intensity, the large-scale environment of atmospheric parameters around these two events was analyzed. Dynamic and thermodynamic variables from ERA5 reanalyses were used.

3. Results and discussion

3.1 Characterization of fog events

The two fog events of April 3 and 30, 2023 over Dakar were detected by the LIDAR Ceilometer and confirmed on the METAR at the Yoff and Diass airport weather stations. The backscatter signal recorded by LIDAR during these two fog events is shown in **Figure 1**. The April 3 event was marked by a high density of fog confined between 0 and 100 m asl. This phenomenon began at around midnight and continued throughout the night, maintaining a high intensity until the early hours of the morning before dissipating at around 10 a.m. at the surface. This high concentration at the surface can be explained by the collapse of the nocturnal boundary layer. During the night, a stable layer of air forms, induced by a temperature inversion. The layer generally dissolves by convection with the appearance of the sun, but it can also remain during the day when solar heating

is not sufficient to disperse the nocturnal boundary layer. However, it is important to note the presence of this signal between 100 and 300 m asl during the day corresponding to maximum sunshine. This could be explained by solar radiation destabilizing the situation at the surface, creating thermals of warm air that rise upwards. The thermal currents continue to rise until their temperature has fallen to the same level as that of the surrounding air. From 5 p.m. onwards, total dissipation was observed across the entire atmospheric column. The configuration of the April 30 event differed from that of April 3 in terms of duration and vertical thickness. The phenomenon started just after 02 a.m., with a significant vertical extension from the surface up to 300 m asl. It lasted three hours before losing its vertical extension and dissipating at the surface, confining itself to between 300 and 400 m asl. This result was confirmed by the horizontal visibility shown in **Figure 2**, where very low visibility (less than 100 m) was observed on April 3 and 30 during the hours of the event. This figure also shows the difference between the two events. On April 3, visibility remained low and constant from 01 a.m. to 11 a.m. On April 30, however, there were two peaks. The strongest peak occurred onset between 2 and 3 a.m., and the secondary peak between 7 and 9 a.m. This type of fog appears to be more dangerous for air transport, as it was reported that at least 4 aircraft were diverted at Diass at the time of the event. And caused the diversion of aircraft due to land at Diass airport. The event of April 30 seems to be less clear-cut, due to the irregular evolution of visibility caused by alternating strengthening and attenuation of weather conditions which favor fog. In fog events such as that of April 3, road transport is often the most affected due to the horizontal reduction in visibility (see **Figure 2**). As illustrated by the heavy collision between a truck and a motorcyclist, which resulted in two deaths on the freeway near Colobane (Dakar, Senegal).

To better characterize these two types of fog, we analyzed surface meteorological parameters such as relative humidity and temperature at the three study sites 1 day before and during the events (**Figure**

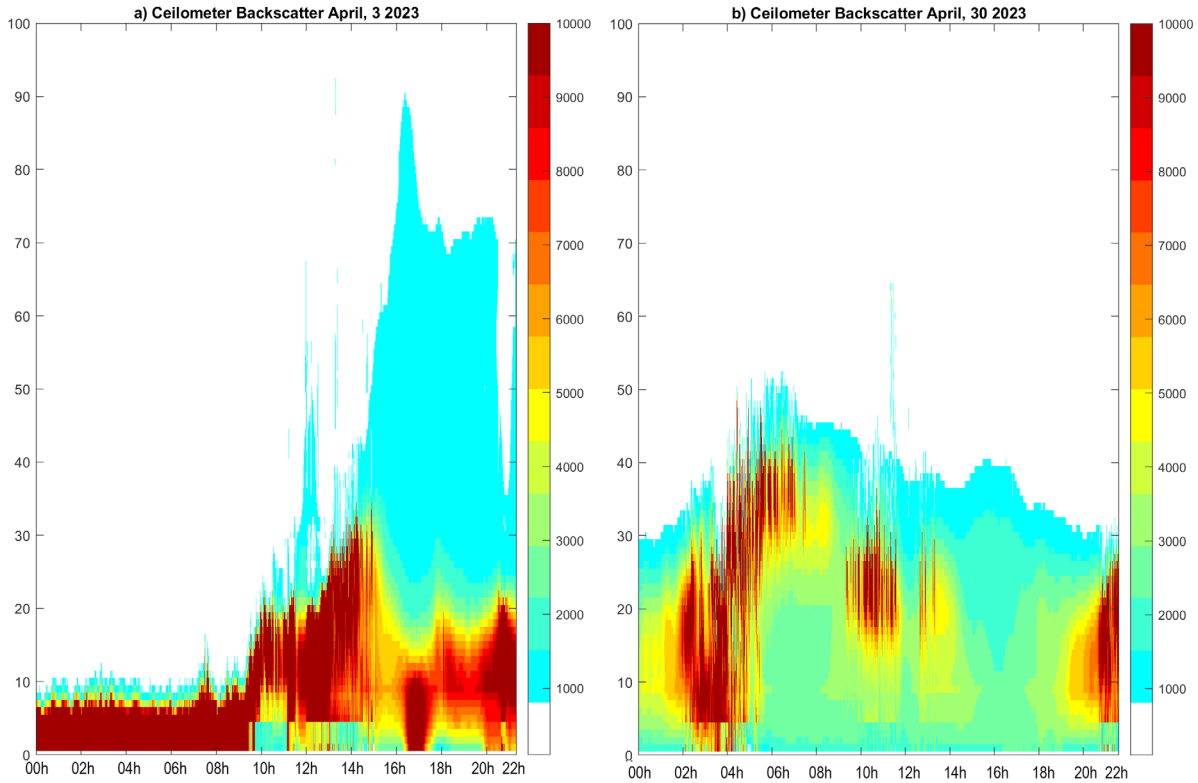

Figure 1. Backscattering of the LIDAR signal for the events of April 3rd and 30th 2023.

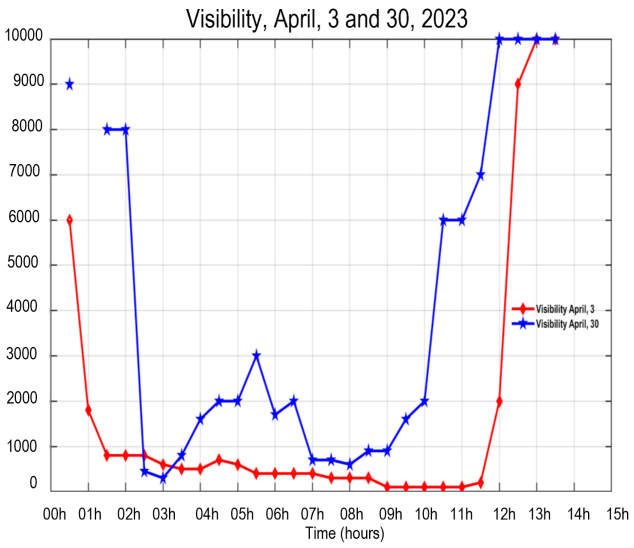

Figure 2. Visibility on April 3 and 30, 2023 in Dakar (METAR AIBD data).

3). This analysis enables us to measure the spatial coherence of these events. The diurnal variation in temperature shows differences between sites the day before the event. The coastal sites of LPAO and Yoff followed a similar pattern, with temperatures reaching 28 and 25 °C respectively at peak sunshine. By contrast, the continental site (Diass airport) showed very marked diurnal temperature variability, with a peak of 35 °C at 12 noon on April 2, the day before the event. This trend was less marked during the April 30 event. However, a slight spatial variation in temperature was observed between these three sites at the time of the fog, with a mean temperature value of around 22 °C. The relative humidity (RH) at the surface measured at all stations exceeded 90% at the time of the events, confirming air mass saturation at all three sites. These results show that a clear drop in temperature, accompanied by an increase in humidity, is conducive to the triggering of fog. However, this condition is not sufficient, given the saturation observed on the night of April 29 without the presence of fog. **Figure 4** shows the wind intensity and direction before and during the events. During the April 3 event, a low-intensity south-westerly wind of around 3 to 10 m/s was observed, bringing moisture to the continent (**Figure 4**). On the other hand, on the eve of the April 30 event, despite saturation combined with a drop in temperature, the high wind intensity inhibited the formation of fog. It took an acceleration of the wind to restore favorable conditions for the April 30th event. Consequently, the impact, location and movement of fog depend on a number of conditions, including wind strength and

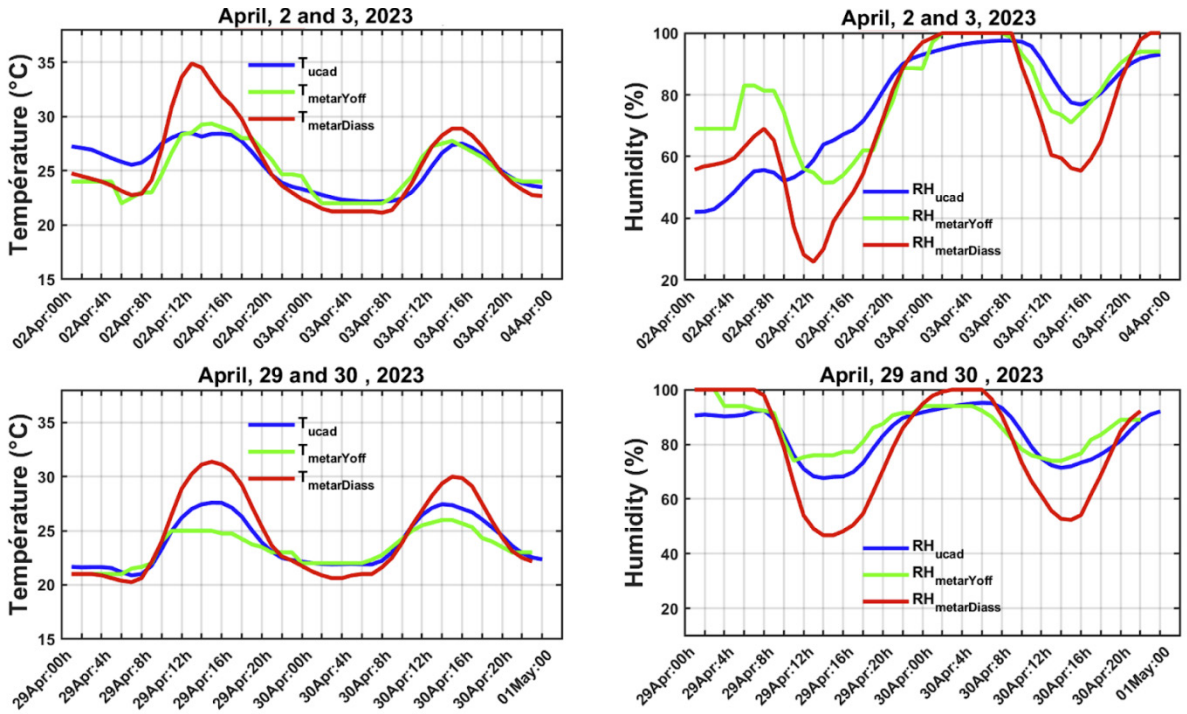

Figure 3. Relative humidity and temperature trends from April 2 to 3 and April 29 to 30, 2023 at Dakar (METAR AIBD data).

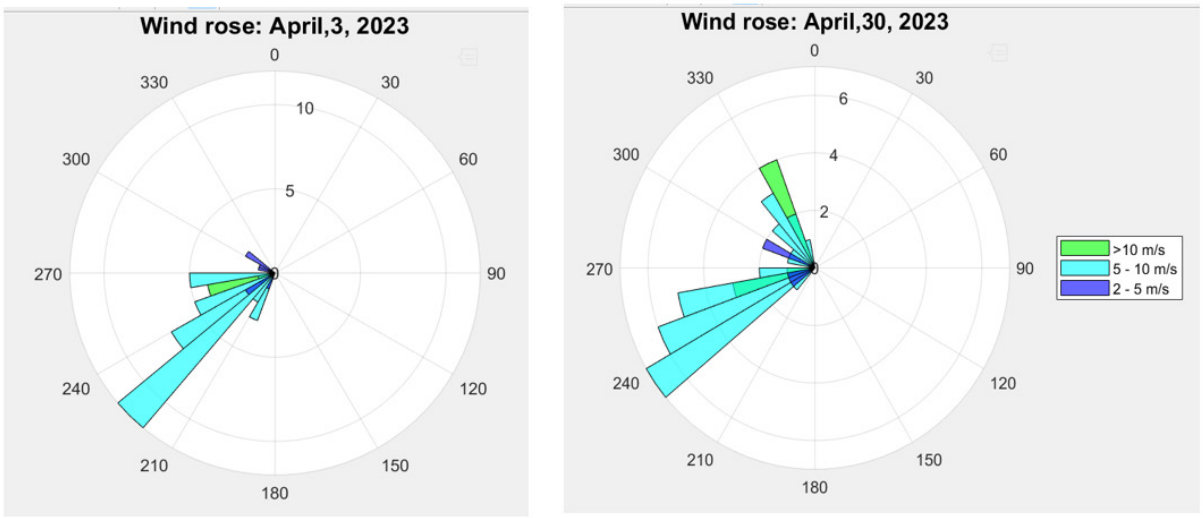

Figure 4. Wind rose from METAR data for Dakar's Blaise Diagne international airport on April 3 and 30, 2023.

direction, ground temperature and humidity. If the wind is strong, fog can dissipate rapidly as the air parcel warms up. On the other hand, if the wind is weak, the fog may persist for longer.

3.2 Analysis of synoptic conditions during fog events

Atmospheric thermodynamic parameters such as minimum sea level pressure (SLP), humidity and winds are factors that influence fog formation, dissipation and frequency of occurrence [31]. SLP can reflect the thermal difference between sea and land, and the spatial distribution of SLP is one of the key factors in fog formation and maintenance. **Figures 5 and 6** show the diurnal variations in SLP anomalies relative to the monthly mean for the month of April 2023 during the April 3 and April 30 fog events. Analysis of these two parameter figures reveals two different patterns. On April 3, a zonal dipole between the continent, more precisely the Sahara (10-25°N; 10°W-10°E), and the northern Senegalese coast was set up during the fog event. The disappearance of this dipole corresponds to the dissipation of the fog at around 11 a.m. to 12 p.m. In addition to this dipole, we observed a decrease in pressure over the Senegalese coast, particularly in our study area, and a strengthening of the Azores anticyclone. This could lead to an influx of moisture from the North Atlantic. This phenomenon, combined with a cooling of the air mass, could explain the persistence of fog until sunrise. For the April 30 event, we observe a dipolar configuration as for April 3, but this time from the south. This meridional dipole is present during the hours of fog, with a strengthening of pressure in the area from the Gulf of Guinea to the equatorial Atlantic, and a decrease in pressure in our study area. Another difference between the two events is the weakening of the Azores anticyclone on April 30, which strengthened during the April 30 event. As a result, moisture transport for the latter event seems to have originated in the equatorial Atlantic, notably in the Gulf of Guinea. Both events could be associated with advection fog. Given the relationship between SLP fields and temperature, this zone of decreasing pressure would correspond to warming. The work of Miller (1958) demonstrated the link between sea surface temperature (SST) and SLP, based on the decrease in surface pressure resulting from warming due to the adiabatic lifting of moist surface air [32]. Saucier's (1955) hypsometric equation illustrates this link, with warm (cold) temperatures resulting in low (high) sea-level pressures [33]. As humidity is a key element in fog formation, advection from a source of moisture is much more favorable than advection from a dry source.

The hovmoller (time-pressure-level) diagrams of relative humidity around our study area (**Figure 7**) show that during the fog event of April 3, the air be-

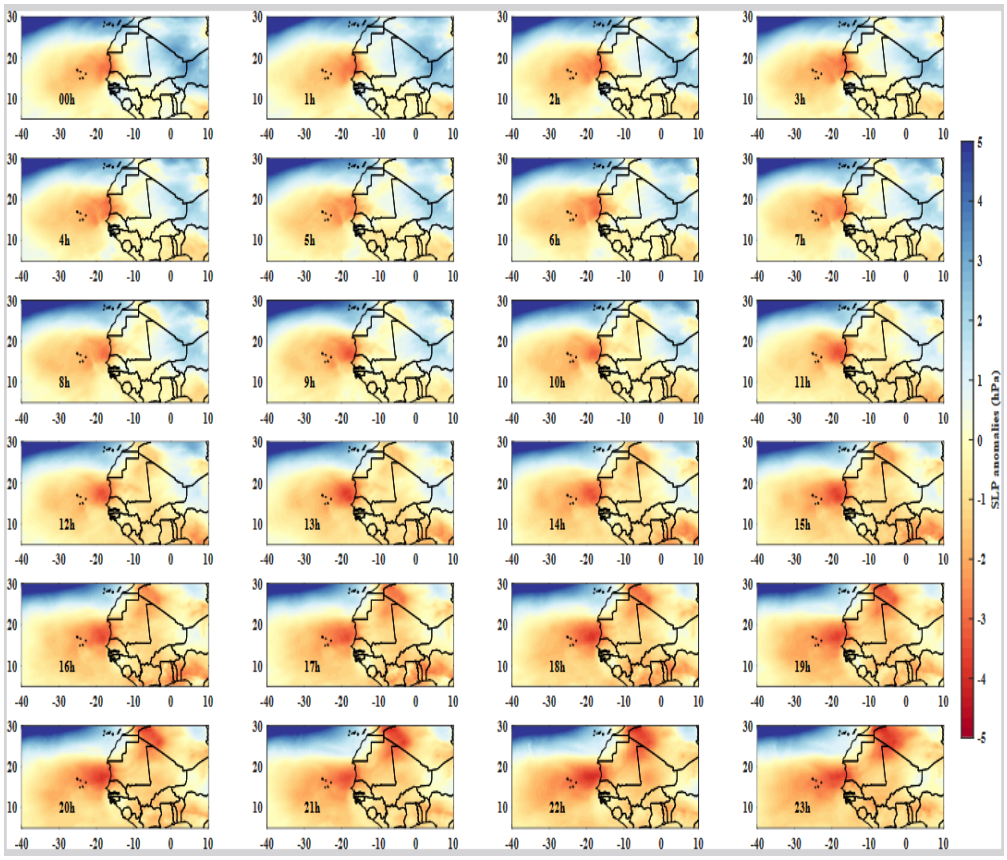

Figure 5. Spatial distribution of SLP anomalies for the event of 3 April 2023 with ERA5 data.

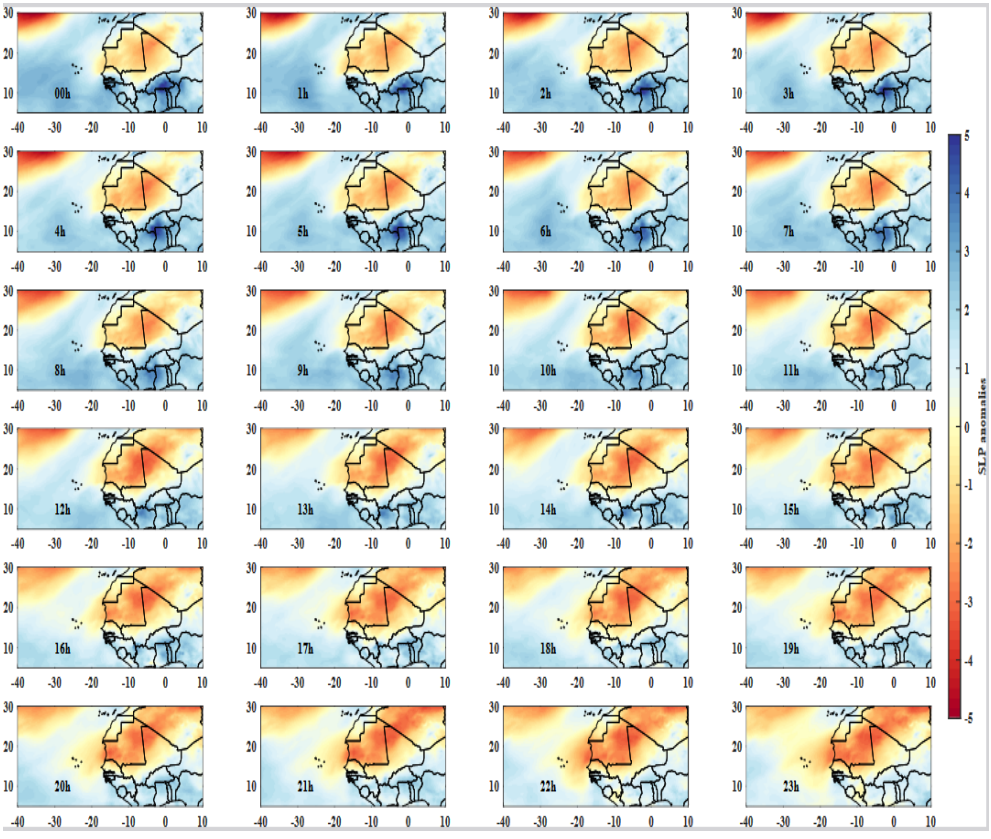

Figure 6. Spatial distribution of SLP anomalies for the event of April 30, 2023 with ERA5 data.

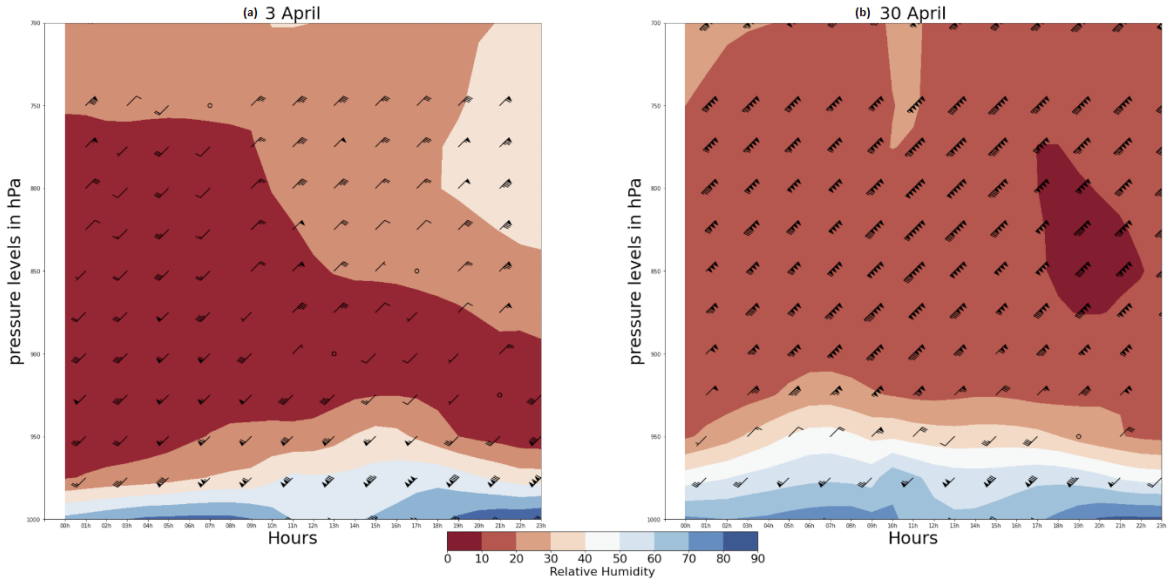

Figure 7. Vertical cross-sections of relative humidity (in color, unit: %), wind field (unit: m/s) for events on April 3 (a) and 30 (b) at different pressure levels.

low 975 hPa (around 300 m) is humid, with humidity levels of between 70% and 80%. This relative humidity increased as the radiation cooled throughout the night and into the morning (between 10 a.m. and 11 a.m.). We also note that relative humidity reached its highest level at the peak of the event (6 a.m. to 11 a.m.), then fell rapidly during the evening (1 p.m. to 5 p.m.). Moreover, during the period of fog formation and persistence, the westerly wind dominated from 1000 to 975 hPa (**Figure 7a**). Moist air from the ocean provided favorable conditions for the formation and persistence of the April 3 fog. Indeed, when relative humidity is high, water begins to condense as temperature drops. This often happens at night, leading to fog formation. Above 975 hPa, the air is dry with a relative humidity of between 10 and 20%. Furthermore, as shown in **Figure 7a**, above 950 hPa, wind speed was low during the global fog process and the prevailing wind direction is from the north-east. The presence of this air tends to confine humidity to the very low layers, favoring the fog's low vertical extension.

For the April 30 event, we observe the same moisture stratification characteristics as for the April 3 fog, but this time the vertical extension is greater (**Figure 7b**). This strong vertical extension of humidity could explain the vertical extension of the April 30 fog. Furthermore, the wind field analysis shows a weak westerly wind in the lower layers and a strong easterly wind in the middle layers (between 950 and 700 hPa) during the hours of the fog event. After the fog event, we note a high wind intensity conducive to fog inhibition. This could explain the short duration of the fog event on April 30.

4. Conclusions

In this work, we studied two fog events observed on April 3 and 30, 2023 over Dakar. Both events were detected by the Ceilometer LIDAR and confirmed on METARs from meteorological stations at Yoff and Diass airports. The backscatter signal recorded by the LIDAR during the April 3 event showed a high density of fog confined between 0 and 100 m asl. This phenomenon began at around midnight and continued throughout the night until the early hours of the morning, before dissipating at around 10 a.m. at the surface. The April 30 event started just after 2 a.m., with a good vertical extension from the surface to 300 m asl and lasted 3 hours.

The characterization of the conditions of formation, persistence and dissipation of the fog events observed on April 3 and 30, 2023 is based on ob-

servations of data from the LPAOSF UCAD-Met network, and the Yoff and Diass METARs. Analysis of surface meteorological parameters such as relative humidity, temperature and wind at 10 m shows that a clear drop in temperature, accompanied by an increase in humidity and a light wind, is conducive to the onset and persistence of fog. In contrast to these conditions, fog dissipation is associated with a strong wind, a decrease in humidity and an increase in temperature due to sunshine. These dissipation conditions are in perfect harmony with the development of the convective boundary layer.

Analysis of the synoptic patterns shows two distinct configurations for the two fog events. Our results highlight a zonal dipole of SLP anomalies between the Sahara and the northern Senegalese coast for the April 3rd event. The April 30 event is characterized by a meridional dipole between the Sahara and the Gulf of Guinea area as far as the equatorial Atlantic. For both events, the fog forms mainly over Dakar under cyclonic or anticyclonic conditions, with a weakening of the pressure around our study area and a strengthening of the pressure over the Sahara. In particular, these conditions are conducive to the formation of advection-radiation fog. Analysis of the hovmoller diagrams of humidity and wind in our study area showed that good vertical extension of humidity combined with a westerly wind in the lower layers play a very important role in the formation and persistence of fog. Furthermore, the presence of dry air and a weak easterly wind above 975 hPa could explain the low vertical extension of the April 3 fog. In addition, the strong wind below 975 hPa could be responsible for the dissipation of the fog, and therefore for the short duration of the April 30 fog event. This analysis can serve as a reference for fog forecasting and early warning. However, given the very limited number of cases, a study over a longer period should enable us to better verify the hypotheses put forward.

Author Contributions

This work was realized in collaboration between all authors. Semou Ndao and Cheikh Modou Noreyni Fall collected and processed data and interpreted the results. They also wrote the first draft of the manuscript. Luis Durán and Abdou lahat Dieng helped to collect Ceilometer's data, contributed ideas and provided valuable comments. Assie Regina Djiguene Diatta collected and processed the METAR data and contributed to interpreting the results and drafting the manuscript. Badara Sane helped to collect Era5 data and provided valuable comments. Amadou Thierno Gaye conceived the idea of the study and supervised the entire work.

Conflict of Interest

The authors declare that there is no conflict of interest.

Acknowledgement

We thank Complutense University of Madrid and interMET for installation and maintenance of Ceilometer's LIDAR CL31. We thank also the European Centre for Medium-Range Weather Forecasts (ECM-WF) for making their Era-5 product available to them and the Agency for the Safety of Air Navigation in Africa and Madagascar (ASECNA) for the METAR data.

References

[1] Fog [Internet]. World Meteorological Organization [cited 2022 Jul 4]. Available from: https://cloudatlas.wmo.int/en/fog.html

[2] Baguskas, S.A., Clemesha, R.E., Loik, M.E., 2018. Coastal low cloudiness and fog enhance crop water use efficiency in a California agricultural system. Agricultural and Forest Meteorology. 252, 109-120.
DOI: https://doi.org/10.1016/j.agrformet.2018.01.015

[3] Fall, C.M.N., Lavaysse, C., Kerdiles, H., et al., 2021. Performance of dry and wet spells combined with remote sensing indicators for crop yield prediction in Senegal. Climate Risk Management. 33, 100331.
DOI: https://doi.org/10.1016/j.crm.2021.100331

[4] Boudala, F.S., Wu, D., Isaac, G.A., et al., 2022. Seasonal and microphysical characteristics of fog at a northern airport in Alberta, Canada. Remote Sensing. 14(19), 4865.
DOI: https://doi.org/10.3390/rs14194865

[5] Zimmer, A., 1930. 'Le brouillard mortel de la vallée de la Meuse': Décembre 1930-Naturalisation de la catastrophe (French) ['Deadly fog of Meuse's valley' (December 1930). Naturalization of the disaster]. Débordements industriels: Environnement, territoire et conflit, edited by Thomas Le Roux and Michel Letté. 115-134.

[6] Gultepe, I., Milbrandt, J.A., Zhou, B., 2017. Marine fog: A review on microphysics and visibility prediction. Marine fog: Challenges and advancements in observations, modeling, and forecasting. Springer: Cham. pp. 345-394.

[7] Kim, C.K., Yum, S.S., 2010. Local meteorological and synoptic characteristics of fogs formed over Incheon international airport in the west coast of Korea. Advances in Atmospheric Sciences. 27, 761-776.

[8] Fu, G., Li, P., Crompton, J.G., et al., 2010. An observational and modeling study of a sea fog event over the Yellow Sea on 1 August 2003. Meteorology and Atmospheric Physics. 107, 149-159.

[9] Heo, K.Y., Ha, K.J., Mahrt, L., et al., 2010. Comparison of advection and steam fogs: From direct observation over the sea. Atmospheric Research. 98(2-4), 426-437.

[10] Wagh, S., Krishnamurthy, R., Wainwright, C., et al., 2021. Study of stratus-lowering marine-fog events observed during C-FOG. Boundary-Layer Meteorology. 181, 317-344.
DOI: https://doi.org/10.1007/s10546-021-00670-w

[11] Ryznar, E., 1977. Advection-radiation fog near Lake Michigan. Atmospheric Environment. 11(5), 427-430.

[12] Fernando, H.J., Gultepe, I., Dorman, C., et al., 2021. C-FOG: Life of coastal fog. Bulletin of the American Meteorological Society. 102(2), E244-E272.
DOI: https://doi.org/10.1175/BAMS-D-19-0070.1

[13] Dione, C., Haeffelin, M., Burnet, F., et al., 2023. Role of thermodynamic and turbulence processes on the fog life cycle during SOFOF3D experiment. Atmospheric Chemistry and Physics Discussions.
DOI: https://doi.org/10.5194/egusphere-2023-1224

[14] Fernando, H.J., Gultepe, I., Dorman, C., et al., 2020. C-FOG: Life of coastal fog. Bulletin of the American Meteorological Society. 1(aop), 1-53.

[15] Bardoel, S.L., Horna Muñoz, D.V., Grachev, A.A., et al., 2021. Fog formation related to gravity currents interacting with coastal topography. Boundary-Layer Meteorology. 181(2-3), 499-521.
DOI: https://doi.org/10.1007/s10546-021-00638-w

[16] Choi, H., Speer, M.S., 2006. The influence of synoptic□mesoscale winds and sea surface temperature distribution on fog formation near the Korean western peninsula. Meteorological Applications: A Journal of Forecasting, Practical Applications, Training Techniques and Modelling. 13(4), 347-360.

[17] Findlater, J., Roach, W.T., McHugh, B.C., 1989. The haar of north□east Scotland. Quarterly Journal of the Royal Meteorological Society. 115(487), 581-608.

[18] Ballard, S.P., Golding, B.W., Smith, R.N.B., 1991. Mesoscale model experimental forecasts of the Haar of northeast Scotland. Monthly Weather Review. 119(9), 2107-2123.

[19] Pilié, R.J., Mack, E.J., Kocmond, W.C., et al., 1975. The life cycle of valley fog. Part I: Micrometeorological characteristics. Journal of Applied Meteorology and Climatology. 14(3), 347-363.

[20] Leipper, D.F., 1994. Fog on the US west coast: A review. Bulletin of the American Meteorological Society. 75(2), 229-240.

[21] Lewis, J.M., Koracin, D., Rabin, R., et al., 2003. Sea fog off the California coast: Viewed in the context of transient weather systems. Journal of Geophysical Research: Atmospheres. 108(D15).

[22] Wong, W.K., Lai, E.S., 2010. Numerical simu-

lation of fog using non-hydrostatic NWP model with third-order turbulence closure. Journal of Hydro-environment Research. 4(2), 131-141.

[23] Diao, X., 1996. Main features of sea fog on Qingdao and its neighbouring sea areas. Marine Science Bulletin-Tianjin. 15, 87-91.

[24] Zhou, B., Du, J., 2010. Fog prediction from a multimodel mesoscale ensemble prediction system. Weather and Forecasting. 25(1), 303-322.

[25] Tsaknakis, G., Papayannis, A., Kokkalis, P., et al., 2011. Inter-comparison of lidar and ceilometer retrievals for aerosol and Planetary Boundary Layer profiling over Athens, Greece. Atmospheric Measurement Techniques. 4(6), 1261-1273.
DOI: https://doi.org/10.5194/amt-4-1261-2011

[26] Guerrero-Rascado, J.L., Costa, M.J., Bortoli, D., et al., 2010. Infrared lidar overlap function: An experimental determination. Optics Express. 18(19), 20350-20369.
DOI: https://doi.org/10.1364/OE.18.020350

[27] Senghor, H., Machu, É., Durán, L., et al., 2020. Seasonal behavior of aerosol vertical concentration in Dakar and role played by the sea-breeze. Open Journal of Air Pollution. 7(9), 11-26.
DOI: https://doi.org/10.4236/ojap.2020.91002

[28] Hersbach, H., Dee, D., 2016. ERA5 Reanalysis is in Production [Internet]. ECMWF. Available from: https://www.ecmwf.int/en/newsletter/147/news/era5-reanalysis-production

[29] Lawrence, M.G., 2005. The relationship between relative humidity and the dewpoint temperature in moist air: A simple conversion and applications. Bulletin of the American Meteorological Society. 86(2), 225-234.

[30] Wang, H., Long, L., Kumar, A., et al., 2014. How well do global climate models simulate the variability of Atlantic tropical cyclones associated with ENSO? Journal of Climate. 27(15), 5673-5692.
DOI: https://doi.org/10.1175/JCLI-D-13-00625.1

[31] Gultepe, I., Tardif, R., Michaelides, S.C., et al., 2007. Fog research: A review of past achievements and future perspectives. Pure and Applied Geophysics. 164, 1121-1159.

[32] Miller, B.I., 1958. On the maximum intensity of hurricanes. Journal of Atmospheric Sciences. 15(2), 184-195.

[33] Saucier, W.J., 1955. Principles of meteorological analysis. University of Chicago Press: Chicago.